AGU PUBLICATIONS

Geophysical Research Letters

RESEARCH LETTER
10.1002/2015GL065287

Special Section:
First Results from the MAVEN Mission to Mars

Three-dimensional structure in the Mars H corona revealed by IUVS on MAVEN

M. S. Chaffin[1], J. Y. Chaufray[2], J. Deighan[1], N. M. Schneider[1], W. E. McClintock[1], A. I. F. Stewart[1], E. Thiemann[1], J. T. Clarke[3], G. M. Holsclaw[1], S. K. Jain[1], M. M. J. Crismani[1], A. Stiepen[1], F. Montmessin[2], F. G. Eparvier[1], P. C. Chamberlain[4], and B. M. Jakosky[1]

[1]Laboratory for Atmospheric and Space Physics, University of Colorado Boulder, Boulder, Colorado, USA, [2]LATMOS/IPSL, Guyancourt, Yvelines/Île-de-France, Guyancourt, France, [3]Center for Space Physics, Boston University, Boston, Massachusetts, USA, [4]NASA Goddard Space Flight Center, Greenbelt, Maryland, USA

Key Points:
- H coronal observations by IUVS confirm previously observed seasonal trends
- Observations require two populations, suggesting either hot H or asymmetries in exobase temperature
- Brightness excess at dawn terminator and winter pole suggest that H can constrain general circulation

Supporting Information:
- Figure S1

Correspondence to:
M. S. Chaffin,
michael.chaffin@colorado.edu

Citation:
Chaffin, M. S., et al. (2015), Three-dimensional structure in the Mars H corona revealed by IUVS on MAVEN, *Geophys. Res. Lett.*, *42*, 9001–9008, doi:10.1002/2015GL065287.

Received 10 JUL 2015
Accepted 23 SEP 2015
Published online 5 NOV 2015

Abstract Loss of water to space via neutral hydrogen escape has been an important process throughout Martian history. Contemporary loss rates can be constrained through observations of the extended neutral hydrogen atmosphere of Mars in scattered sunlight at 121.6 nm. Historically, such observations have been interpreted with coupled density and radiative transfer models, inferring escape fluxes from brightness profiles gathered by flybys, orbiters, and telescope observations. Here we demonstrate that the spherical symmetry assumed by prior analyses cannot reproduce observations by the Imaging Ultraviolet Spectrograph (IUVS) on the Mars Atmosphere and Volatile EvolutioN (MAVEN) mission. We present unique observations of the Mars H corona to large radial distances and mapping results from initial MAVEN science at Mars. These observations represent the first detection of three-dimensional structure in the H corona of Mars, with implications for understanding the atmosphere today and the loss of H to space throughout Martian history.

1. Introduction

At large distances, every planetary atmosphere is surrounded by a diffuse corona of atomic hydrogen, visible in scattered sunlight at 121.6 nm, the Lyman alpha line of neutral hydrogen. The Mars Atmosphere and Volatile EvolutioN mission (MAVEN) [*Jakosky et al.*, 2015] carries an Imaging Ultraviolet Spectrograph (IUVS) [*McClintock et al.*, 2014] designed in part to detect this wavelength. Observations of coronal brightness indirectly reveal the density structure of H and can be used to derive the escape rate of neutral hydrogen to space, a key control on atmospheric photochemistry [*Nair et al.*, 1994; *Zahnle*, 2008; *Fox*, 2015], with the potential to have removed perhaps as much as 85% of the initial planetary water inventory [*Villanueva et al.*, 2015]. Atomic and molecular hydrogen in the thermosphere and corona influence the ionospheric chemistry of protonated species [*Fox*, 2003; *Matta et al.*, 2013; *Fox*, 2015], can affect the escape of energetic neutral atoms [*Holmström*, 2006], and together with coronal oxygen may decelerate the solar wind upstream of the bow shock via mass loading [*Verigin et al.*, 1991; *Dubinin et al.*, 2000]. Determining the structure and variability of the corona is therefore important not only for reconstructing the history of water loss but also for understanding the overall structure of the Mars atmosphere.

Historically, observations of the Mars H corona by flyby and orbiter missions, including Mariner 6, 7, and 9 [*Anderson and Hord*, 1971; *Anderson*, 1974], Mars 2 and 3 [*Dostovalov and Chuvakhin*, 1973], Mars Express [*Chaufray et al.*, 2008; *Chaffin et al.*, 2014], and Rosetta [*Feldman et al.*, 2011], as well as observations from Earth-orbiting space telescopes [*Levine et al.*, 1978; *Clarke et al.*, 2014; *Bhattacharyya et al.*, 2015] have been interpreted using coupled physical density and radiative transfer models. These analyses almost always assumed a fixed exobase, as well as an isotropic and Maxwellian Chamberlain exosphere [*Chamberlain*, 1963] for computing the density of the exosphere and corona and employed the assumptions of *Thomas* [1963] to simulate the brightness of the optically thick corona (vertical line center $\tau \sim 10$) in scattered sunlight. (A notable exception is the introduction by *Chaufray et al.* [2008] of a nonself-consistent spherically symmetric hot component, similar to that detected at Venus [*Anderson*, 1976] into modeled densities.) The simplicity of these models was justified by the generally excellent correspondence between the data and the model within the estimated data uncertainties, and a lack of comprehensive global observations of the corona, as most previous analyses were limited to one-dimensional brightness profiles widely spaced in time.

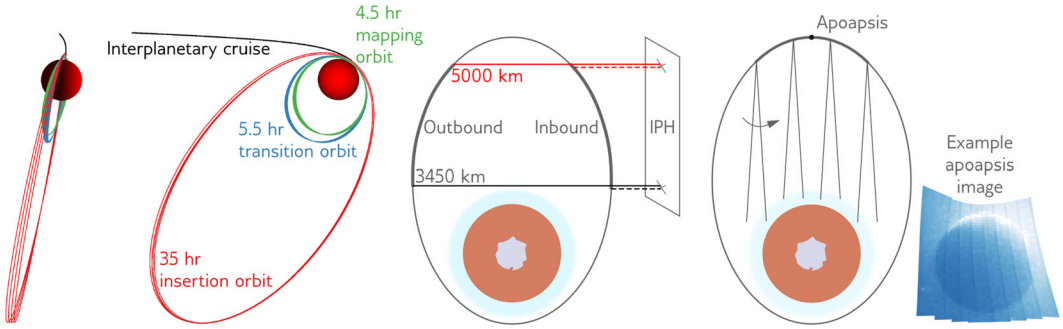

Figure 1. Summary of IUVS coronal observation modes. (left) Illustration of MAVEN insertion, transition, and mapping orbit in the first weeks after MAVEN arrival at Mars on 21 September 2014. The 35 h insertion orbit achieved very high altitudes, allowing imaging of the distant corona not possible from MAVEN's mapping orbit. (middle and right) In its mapping orbit, IUVS observes the corona on the outbound and inbound legs with coronal scans pointed inertially across the orbit, which inevitably observe interplanetary hydrogen (IPH) as a background. Surrounding apoapsis, a map is made of the full disk, using a scan mirror to sweep out one dimension of the image (in and out of the page), with spacecraft motion supplying the orthogonal direction. These data can be rotated and overlaid to produce a circular planet image.

With MAVEN and IUVS at Mars, the Mars H corona is more densely sampled in both space and time than ever before. Figure 1 describes the modes IUVS uses to probe the H corona. A sequence was developed for MAVEN's insertion orbit, which carried the spacecraft to much larger distances from the planet than the current and future mapping orbit. Insertion observations probed the corona to line of sight tangent point distances more than 10 Mars radii away from the planet, revealing the outer corona with unprecedented signal to noise. In its mapping orbit, IUVS observes the corona with two modes of operation: inertially pointed coronal scans, which generate one-dimensional profiles on the outbound and inbound legs of the orbit, and apoapsis maps, which generate a two-dimensional image of the disc using spacecraft and scan mirror motion.

To interpret these IUVS observations, we compare observed intensities with a coupled Chamberlain/Thomas model for coronal brightness, as described in *Chaufray et al.* [2008] and *Chaffin et al.* [2014]. The model has two free parameters: the number density and Maxwellian temperature of hydrogen at an assumed exobase altitude of 200 km. The Chamberlain exosphere model assumes a uniform temperature and density at all exobase locations, with H densities spherically symmetric around Mars. Thermospheric diffusion below the exobase is implemented by using an analytic temperature profile as described by *Krasnopolsky* [2002]. To perform the radiative transfer, the Thomas model assumes Doppler line profiles, a flat solar line, and complete frequency redistribution, resulting in photon scattering rates which are azimuthally symmetric about the Mars-Sun line. Because simulating the brightness of the atmosphere is computationally intensive, precomputed source functions are used, which are integrated along the spacecraft line of sight to generate simulated brightness profiles for comparison with spacecraft data. These source functions were computed for a range of exobase densities and temperatures incorporating all previously published retrievals of the exobase density and temperature, $n_H = 10^4 - 10^6$ cm^{-3}, $T = 100 - 1500$ K, at a sufficiently high resolution to support bilinear interpolation. In many cases, we fit the model to the data using chi-square minimization, using estimated data uncertainties that are largely photon-noise dominated.

IUVS brightnesses were calibrated using UV bright stars, scaled by instrument geometric factors appropriate for extended source observations. The resulting calibration retains a ±25% systematic uncertainty in sensitivity in the interval 108–190 nm and is especially uncertain for observations at Lyman alpha, where calibration against stellar reference spectra is difficult due to Lyman alpha extinction and scattering by interstellar and interplanetary hydrogen. The current calibration results in Lyman alpha irradiances that are systematically brighter than prior observations of the IPH and Mars corona. These coronal brightnesses cannot be encompassed within the precomputed model parameter space, requiring physically unrealistic hydrogen temperatures in excess of 1500 K, the temperature at which the most probable Maxwellian hydrogen atom velocity equals Mars escape velocity. If these temperatures were correct, the H observed would have to be in thermodynamic disequilibrium with the bulk thermosphere and escaping hydrodynamically, a very unlikely situation. A better explanation for the too large brightnesses is that IUVS calibrated Lyman alpha brightnesses are systematically too high.

To assess the instrument calibration, we employ near-simultaneous observations of the H corona with IUVS and the Hubble Space Telescope (HST), coincident with the close passage of Comet Siding Spring by the planet in October 2014. Comparison indicates that IUVS brightnesses are larger by a factor near 25% relative to HST and therefore to a large collection of prior ultraviolet instruments, as discussed by *Snow et al.* [2013]. In the present work we adopt a spatially, spectrally, and temporally constant model scale factor of 1.25, multiplying all model brightnesses by this factor before comparison with the data. This scale factor, combined with the optically thick nature of the scattering, makes retrieval of exobase densities, temperatures, and escape rates unreliable at the present time, and so we do not report our retrieved parameters, as these may be uncertain by a factor of 5 or more. Instead, the results we report on here are purely morphological, making them insensitive to the instrument absolute calibration. All figures shown use the nominal IUVS calibration, with models scaled up by the model scale factor of 1.25. The figures therefore likely overestimate the coronal brightness. We use measurements from MAVEN's Extreme UltraViolet Monitor (F. G. Eparvier, An Extreme Ultra-Violet Monitor (EUVM) for the Mars Atmosphere and Volatile EvolutioN mission (MAVEN), submitted to *Space Science Reviews*, 2015) to supply the solar Lyman alpha brightness, and for display purposes to scale all observations to the same input brightness, removing an approximate 10% variability in coronal brightness due to solar rotation. Finally, small defects in the instrument flat field amounting to a 10% sensitivity variation along the slit have not been removed, with minimal effect on the results shown here. These flat-field variations are most apparent in apoapsis maps.

2. Insertion Orbit Observations

IUVS observations of the corona during the 35 h insertion orbit spanned the entirety of the instrument's two fields of regard, using continuous scan mirror motion to probe the corona along all accessible lines of sight throughout the first three orbits of MAVEN around Mars. To combine data gathered in all three orbits into a single image and avoid contamination from observations gathered near Mars while deeply embedded in the corona, instrument data gathered at a radial distance of more than $10\,r_{\mathrm{Mars}}$ were selected, resulting in Lyman alpha intensities observed along more than 400,000 lines of sight. Each line of sight was binned in a two-dimensional angular coordinate system centered on Mars, with one axis toward the Sun. Angular bin sizes were set at $r_{\mathrm{Mars}}/20$, using the angular size of Mars appropriate to each spacecraft location. Binned intensity values were then averaged. The result of this process is shown in Figure 2, which represents an angular map of the sky as seen by MAVEN during its insertion orbit. At apoapsis during the insertion orbit, Mars subtended just over 10° on the sky. The gross structure of the corona is similar to that seen with the Hubble Space Telescope [*Clarke et al.*, 2014], indicating a decrease in coronal brightness with increasing solar zenith angle.

To understand whether the corona in these images is well fit by a Chamberlain exosphere, the coupled physical and radiative transfer model was fit against all lines of sight gathered in all three orbits simultaneously. The best fit was obtained by chi-square minimization of the two-parameter model with respect to the intensity observed, incorporating estimated uncertainties in the data. Because the observations cover such a wide region on the sky, the slowly varying structure of interplanetary hydrogen emission [*Quémerais et al.*, 2013] is imprinted below that of the corona. This structure is modeled with a fully integrated IPH background model based on that of *Lallement et al.* [1985], computing the IPH intensity observed along the spacecraft line of sight and the extinction imposed by the corona, incorporating the Doppler shift of Mars and the spacecraft relative to the line of sight IPH velocity. The IPH brightness of 200–1000 Rayleigh is much smaller than the brightness of most of the corona, contributing a substantial fraction of the total brightness only at the edges of the corona image. After fitting, the resulting best fit model is a simulated data set with the same size and geometrical sampling as the observations. In order to compare the model and the data and guard against potential artifacts, the best fit was processed identically to the original data, resulting in an image of the model corona.

The structure of the model corona is more confined in radius and distributed in solar zenith angle than the data. The model brightness structure, resulting from a pure Chamberlain exosphere, is not shared by the data, which appears more concentrated or collimated in the sunward direction than the model. Increasing the temperature of the model does not change its characteristic shape, suggesting that the Mars corona is not well represented by Chamberlain theory.

The relative deviation of the model and the data reveals several difficulties with the fit. First, the modeled disk intensities are too low, likely due to inaccuracies in the model thermosphere temperature or transport

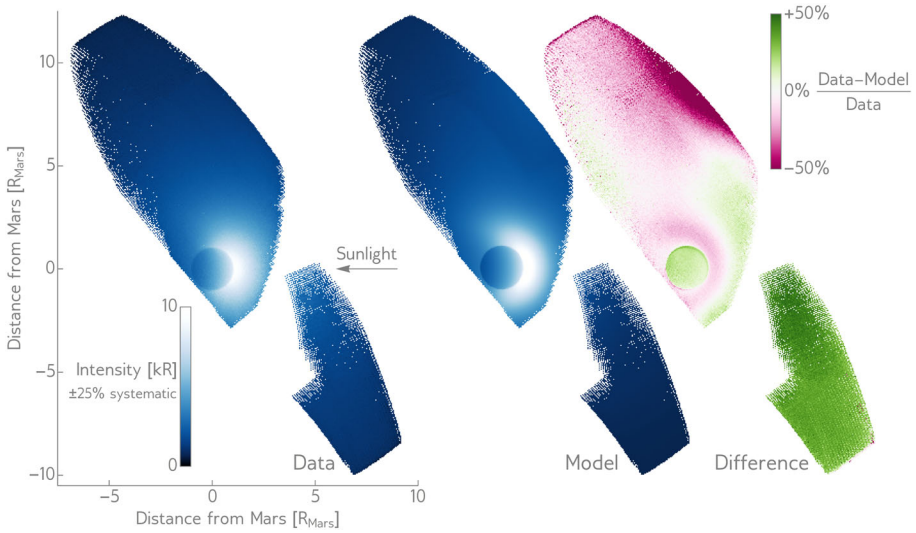

Figure 2. IUVS insertion orbit observations of the Mars H corona. (left) A synthetic image of the Mars corona constructed via coaddition of ~400,000 line of sight observations through the corona made over the course of about 4 days following MAVEN's Mars orbit insertion. (middle) The best fit Chamberlain/Thomas model to the entire insertion orbit data set, processed identically to produce a comparison synthetic image on the same scale. (right) Normalized difference of data and model, revealing that the model overpredicts the data in the inner corona but underpredicts it in the outer corona. This discrepancy between the model and the data indicates that a single-population exosphere is insufficient to support the observed coronal intensities. Intensities are likely systematically too bright by 25%; see discussion in text.

(adopted from *Krasnopolsky* [2002] as briefly described above) which underpredict the thermospheric hydrogen abundance relative to the data. Second, the model corona is too bright near the planet and too dim far away, indicating that the model is balancing deviations from the data near the planet against those in the distant corona. This indicates that the data would be better fit with two populations: one that dominates near the planet and another that dominates farther away. This requirement for two populations is a clear argument either for a global hot hydrogen population at Mars or for spatial temperature asymmetries in the corona, with high densities and small-scale heights and temperatures on the nightside at low altitude, supplemented by larger-scale heights at high altitude resulting from transport of H across the limb from the dayside. Both explanations are incompatible with the Chamberlain physical density model: more detailed modeling is required to capture the three-dimensional structure of the corona, especially in order to determine an accurate escape rate. Finally, the excess of the model relative to the data at the top of the image indicates that the relatively simple IPH model (plotted separately in the supporting information Figure S1) is not accurately reflecting the background intensities, requiring more sophisticated modeling in future work. These large relative deviations represent small absolute variations at the large distances from the planet where the IPH contribution is significant: inaccuracies in the IPH model are less important close to the planet, where MAVEN gathers its mapping data.

3. Coronal Scans

Coronal scans from the first 4 months of MAVEN operations are shown in Figure 3. IUVS gathers H coronal scans every fourth spacecraft orbit, when the instrument controls its orientation and is in low-resolution mode. The MAVEN orbit was designed to precess around Mars so that in situ instruments can sample a wide range of solar latitudes and longitudes at periapsis. For this reason, coronal scans made along the sides of the orbit also sweep through different locations in the corona with time. At the beginning of the MAVEN mission in late 2014, IUVS coronal scans looked toward the nightside of the planet across the evening terminator in the southern hemisphere. Over the next 6 months, these scans swept around Mars as seen from below, passing south of the subsolar point. By the beginning of March 2015, the coronal scans were oriented toward the southern dayside across the dawn terminator.

The brightness observed in the coronal scans is commensurate with the portions of the corona observed, increasing in brightness as the instrument line of sight moves into the dayside corona, with the brightest

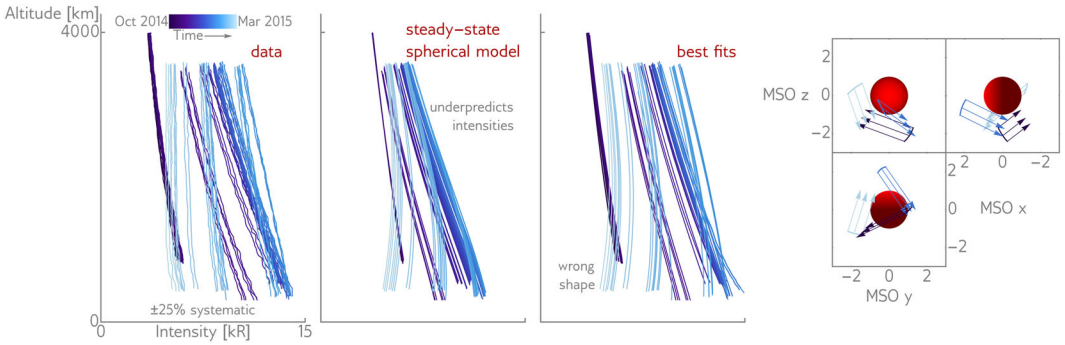

Figure 3. IUVS coronal scans, October 2014 to March 2015. All panels share the same color scale (indicated at the top left), with darker colors for observations made early in the mission and lighter colors from more recent scans. (first panel) Data from outbound IUVS coronal scans. (second panel) Steady state model profiles, using best fit parameters to the earliest set of limb scans to simulate brightness for all scans, indicating that a model that does not change with time cannot reproduce observed brightnesses. (third panel) Best fit Chamberlain/Thomas model to each scan individually, incorporating time variations but assuming spherical symmetry. Qualitatively incorrect shapes for the most recent scans indicate that the corona is not spherically symmetric. (fourth panel) Geometry of the observations, indicating the evolution of the MAVEN orbit over the time period shown. Arc shows spacecraft positions during the observation, with arrows pointing along the instrument line of sight, which lies in the orbit plane. Early observations were made toward the nightside from near the afternoon terminator; over the subsequent months the sampling region passed through local noon, with the most recent observations shown made toward the dayside across the dawn terminator. Intensities are likely systematically too bright by 25%; see discussion in text.

observations occurring near the subsolar point in the middle of the observation set. For later observations, the intensity profiles get dimmer but become increasingly shallow, with nearly vertical shapes at the end of the observation period when the instrument is looking across the dawn terminator.

To aid interpretation of these profiles, two model case studies were computed. First, the Chamberlain/Thomas model was fit to the earliest coronal profiles, taken in October. The best fit to the early observations was used to compute theoretical intensities for the observation geometry of all other coronal scans. This simulation set tests the "steady state" null hypothesis that there is no latitude, longitude, or temporal variability present in the corona. Second, the model was used to determine the best fit parameters for each observation independently. This case study can identify temporal but not geographical variation, as the underlying physical density model is spherically symmetric. This second test determines whether the coronal profiles can be fit with a time-varying exosphere only or if spatial variation is also required.

The results of the model case studies are shown side by side with the data in Figure 3. The steady state model does an adequate job of fitting the earliest observations by design, but for later observations the fit is increasingly poor, with the worst fit near the subsolar point on the dayside. The slopes of the model on the dayside are uniformly shallower than the data, a problem that is only exacerbated for the latest observations, where the model profile shapes are qualitatively incorrect. This indicates that there is substantial temporal or spatial variability in the corona not reflected by a steady state model. (The model shapes, which increase in intensity at middle altitudes, are not wrong. While density decreases monotonically with altitude, the optically thick nature of the corona and the fact that the spacecraft is embedded deep in the corona means that the intensities can increase with tangent altitude as the spacecraft views more illuminated regions.)

One possible explanation for the temporal variation observed in the corona is the evolution uncovered by Mars Express [*Chaffin et al.*, 2014] and HST [*Clarke et al.*, 2014; *Bhattacharyya et al.*, 2015], which affects the extent of the corona on seasonal timescales. A second possibility is a contribution from potential hot hydrogen to the exospheric profiles, which could act to inflate the scale height on the dayside only, with a maximum effect near perihelion when solar forcing is strongest.

Allowing the model to perform a best fit to each observation improves the match to the data, greatly increasing the scale heights on the dayside near the midpoint of the observations. The model still does a poor job of fitting the shape of the profiles for the latter half of the observations, predicting convex profiles while the data are extremely shallow and concave. This indicates that temporal variability alone is not enough to explain the

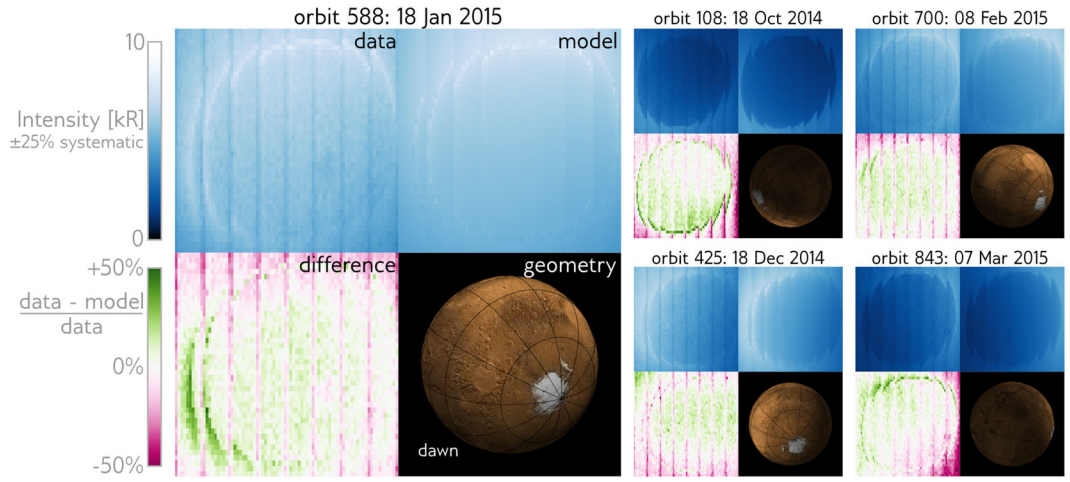

Figure 4. IUVS apoapsis maps. (left) Large image set shows (clockwise from top left) IUVS observations, best fit model to the observations, observation geometry (white feature is the Martian south polar cap), and relative difference of data and model. (right) Four additional image sets, indicating that the model does an effective job of fitting dayside observations but fails to accurately reproduce high intensities at the dawn terminator and in the vicinity of the winter pole. By contrast with the example in Figure 1, in these images all of the data are viewed at once with all swaths side by side. This results in some regions of the corona and planet appearing multiple times. Intensities are likely systematically too bright by 25%; see discussion in text.

observations: the underlying model is incorrect, and escape rates computed from the model do not reflect reality. The model deficiency is likely due to the assumption of spherical symmetry of the hydrogen density distribution. The shallow slopes observed looking across the dawn terminator indicate either that there is much higher escape occurring at dawn (i.e., a much higher temperature at dawn than on the bulk of the dayside) or more likely that this region is a location of significant transport from the remainder of the atmosphere. Either possibility would act to increase the density and therefore brightness of the corona at high altitudes relative to low altitudes.

4. Apoapsis Maps

Apoapsis disc maps complete the means IUVS has of constraining the H corona. At the top of its orbit, IUVS is oriented downward toward the planet and the instrument field of view is scanned across the disc in two dimensions. One dimension is mapped by the instrument scan mirror, and the second covered with spacecraft drift. In total, eight passes across the planet are made, referred to as swaths. The data gathered near apoapsis can be transformed into a Mars-centric frame and overlapped; a circular planet image results (see Figure 1).

IUVS gathers apoapsis images in each orbit around Mars, at 4 times the cadence of the coronal scans for hydrogen. The images are limited in their ability to assess the full H corona, because Mars subtends more than 40° even when the spacecraft is farthest from the planet and because the instrument is still deeply embedded in the corona at its $3R_{Mars}$ apoapsis. Nevertheless, disk and near-limb science can be performed with these images, whose greatest tangent distance from Mars approaches 1000 km.

Figure 4 shows several apoapsis observation sets, including one from mid-January with a clear view of the corona near the dawn terminator. Observations which image the dawn terminator show a brightness excess in the data with respect to the model, indicating that the Chamberlain model employed is significantly under-predicting the abundance of hydrogen in this region, supporting the idea that transport or local production of hydrogen is increasing densities at the dawn terminator. The feature is persistent for weeks and is visible as long as the dawn terminator is aligned with the limb. This suggests that the bulge results from long-lived processes operating in the atmosphere, such as seasonal thermospheric circulation.

In the remaining apoapsis images, the model is often forced to strike a balance between disk and coronal intensities. This indicates that the population supplying the corona is not the same as that imaged on the disk, a likely consequence of supply by the hotter dayside contributing more to coronal densities at high altitude. The model is particularly bad at fitting images that mostly observe the nightside of the planet. In these cases the observations may be sensitive to the likely density imbalance between the dayside and nightside of the

planet, resulting from the thermospheric general circulation. A density imbalance between the hemispheres would force the model to select an intermediate value, between those actually present on the dayside and the nightside. This is particularly noticeable in the image sets gathered in early March 2015, parts of which image near north polar night, the focus of hemispheric circulation and downwelling at this time of the Martian year [*Chaufray et al.*, 2015; *Valeille et al.*, 2009]. This circulation acts to increase the density of hydrogen in the polar night, resulting in model underprediction (green) of the densities toward the north pole.

5. Discussion

Simulations of the 3-D distribution of hydrogen in the upper atmosphere provide context for IUVS observations. Using a general circulation model of the thermosphere and ionosphere, *Chaufray et al.* [2015] simulated the density and temperature distributions of hydrogen at the exobase at several seasons of the Martian year. In part, the study compared density profiles of coronal hydrogen resulting from the 3-D model with 1-D Chamberlain models using local conditions. The authors found that one-dimensional calculations using the local hydrogen density and temperature track the three-dimensional hydrogen distribution below 1000 km but depart significantly at higher altitude. In the highest regions of the corona the three-dimensional simulations are isotropic: at these altitudes the hydrogen in the corona is sourced from the entire thermosphere and tracks the mean thermospheric density and temperature. At lower altitudes, the temperature of each region has more of an effect, resulting in a density enhancement below 1000 km at dawn at equinox.

In Chaufray's simulations, the location of the density enhancement varies with season, based on the prevailing thermospheric winds. At equinox, a large enhancement at dawn is produced, but near solstice the bulge is concentrated on the nightside. The IUVS coronal and apoapsis scans observed the dawn limb in January–February 2015, just after southern summer solstice. At this season, the thermosphere model predicts that no H bulge should be present at the terminator. The enhanced brightness of this region in IUVS observations relative to spherically symmetric models suggests that a dawn bulge is present, in contradiction of the model prediction. This indicates that current 3-D thermosphere models may be missing important physics relevant to production and transport of hydrogen. An overabundance of H at the dawn terminator would affect the ionospheric and thermospheric chemistry active in this region, as indicated by models of the effect of varying atomic and molecular hydrogen abundance on the abundance of protonated species [*Fox*, 2003; *Matta et al.*, 2013; *Fox*, 2015].

6. Conclusions and Future Work

The MAVEN data sample the Mars H corona more completely than any previous mission or observational campaign. For the first time, the high cadence and broad geographical coverage of these data enable a comprehensive overhaul of models for neutral H escape at Mars, demonstrating that a single-temperature Chamberlain exosphere model is insufficient to support the observations. Inconsistent intensities in the near and far corona observed in MAVEN's 35 h insertion orbit, together with anomalous intensity values observed near the dawn terminator and across the nightside, suggest that there are significant nonthermal and nonspherically symmetric phenomena affecting the population of the corona and affecting the escape rate of hydrogen to space. Interestingly, these asymmetries appear different than those predicted from 3-D thermosphere-exosphere simulations.

To fully account for the observed coronal intensities, more sophisticated models of the hydrogen thermosphere and exosphere are required. The inability of the Chamberlain/Thomas model to simultaneously account for the near and far corona observed in MAVEN's insertion orbit, as well as the three-dimensional structure and dawn bulge revealed by coronal scans and apoapsis images, suggests that the Mars corona is not well approximated by Chamberlain theory. To fit the IUVS observations properly, models will likely require increased densities of hydrogen at dawn and may require a dayside contribution from hot, nonthermal hydrogen. This may have a large impact on estimates of the current thermal escape rate of hydrogen from Mars: all previous estimates based on spacecraft data have used these models to estimate escape rates. A more accurate treatment of the three-dimensional structure of the corona is underway, including an exploration of the quantitative impact of this structure on derived escape rates. Exploring the space of additional parameters required by the model to obtain a satisfactory fit to the data will constitute the majority of the MAVEN data analysis. With its high-cadence and high-quality data, MAVEN's IUVS will constrain the structure of the corona and its variability more fully than ever before.

Acknowledgments
This work and the MAVEN project are supported by NASA through the Mars Exploration Program. The data used (all IUVS L1C coronal lyman alpha data from mission start to 10 March 2015 tagged "early," "outbound," and "apoapse" with version/revision tag v02_r01, as well as EUVM Lyman alpha channel data) are archived in NASA's Planetary Data System. The IUVS data used are accessible at the following link: http://atmos.nmsu.edu/data_and_services/atmospheres_data/MAVEN/maven_iuvs.html. Thanks are owed to the many engineers on the MAVEN team who worked to enable observations of the corona within hours of the spacecraft's arrival at Mars. Eric Quemerais provided a version of his IPH brightness modeling code used to simulate the IPH underlying Mars coronal brightness. Roger Yelle provided useful discussion and motivation to search for geographical effects. M.S. Chaffin developed the H corona model with partial assistance from NASA Earth and Space Science Fellowship grant 11-Planet11F-0060. J.-Y. Chaufray is supported by the Centre National d'Etudes Spatiales. A. Stiepen is supported by the Belgian American Educational Foundation and the Rotary District 1630.

The Editor thanks two anonymous reviewers for their assistance in evaluating this paper.

References

Anderson, D. E. (1976), The Mariner 5 ultraviolet photometer experiment: Analysis of hydrogen Lyman alpha data, *J. Geophys. Res.*, *81*(7), 1213–1216.

Anderson, D. E., Jr. (1974), Mariner 6, 7, and 9 ultraviolet spectrometer experiment: Analysis of hydrogen Lyman alpha data, *J. Geophys. Res.*, *79*, 1513–1518.

Anderson, D. E., Jr., and C. W. Hord (1971), Mariner 6 and 7 ultraviolet spectrometer experiment: Analysis of hydrogen Lyman-alpha data, *J. Geophys. Res.*, *76*, 6666–6673.

Bhattacharyya, D., J. T. Clarke, J.-L. Bertaux, J.-Y. Chaufray, and M. Mayyasi (2015), A strong seasonal dependence in the Martian hydrogen exosphere, *Geophys. Res. Lett.*, *42*, doi:10.1002/2015GL065804.

Chaffin, M. S., J.-Y. Chaufray, I. Stewart, F. Montmessin, N. M. Schneider, and J.-L. Bertaux (2014), Unexpected variability of Martian hydrogen escape, *Geophys. Res. Lett.*, *41*, 314–320, doi:10.1002/2013GL058578.

Chamberlain, J. W. (1963), Planetary coronae and atmospheric evaporation, *Planet. Space Sci.*, *11*, 901–960.

Chaufray, J. Y., J. L. Bertaux, F. Leblanc, and E. Quémerais (2008), Observation of the hydrogen corona with SPICAM on Mars Express, *Icarus*, *195*, 598–613.

Chaufray, J.-Y., F. Gonzalez-Galindo, F. Forget, M. Lopez-Valverde, F. Leblanc, R. Modolo, and S. Hess (2015), Variability of the hydrogen in the Martian upper atmosphere as simulated by a 3D atmosphere-exosphere coupling, *Icarus*, *245*, 282–294.

Clarke, J. T., J.-L. Bertaux, J. -Y. Chaufray, G. R. Gladstone, E. Quemerais, J. K. Wilson, and D. Bhattacharyya (2014), A rapid decrease of the hydrogen corona of Mars, *Geophys. Res. Lett.*, *41*, 8013–8020, doi:10.1002/2014GL061803.

Dostovalov, S. B., and S. D. Chuvakhin (1973), On the distribution of neutral hydrogen in the upper atmosphere of Mars, *Cosmic Res.*, *11*, 687.

Dubinin, E., K. Sauer, M. Delva, R. Grard, S. Livi, R. Lundin, A. Skalsky, K. Schwingenschuh, K. Szego, and J.-G. Trotignon (2000), Multi-instrument study of the upstream region near Mars: The Phobos 2 observations, *J. Geophys. Res.*, *105*(A4), 7557–7571.

Feldman, P. D., et al. (2011), Rosetta -Alice observations of exospheric hydrogen and oxygen on Mars, *Icarus*, *214*, 394–399.

Fox, J. L. (2003), Effect of H_2 on the Martian ionosphere: Implications for atmospheric evolution, *J. Geophys. Res.*, *108*(A6), 1223, doi:10.1029/2001JA000203.

Fox, J. L. (2015), The chemistry of protonated species in the Martian ionosphere, *Icarus*, *252*, 366–392.

Holmström, M. (2006), Asymmetries in Mars' exosphere, *Space Sci. Rev.*, *126*(1–4), 435–445.

Jakosky, B. M., et al. (2015), The Mars Atmosphere and Volatile EvolutioN (MAVEN) mission, *Space Sci. Rev.*, doi:10.1007/s11214-015-0139-x.

Krasnopolsky, V. A. (2002), Mars' upper atmosphere and ionosphere at low, medium, and high solar activities: Implications for evolution of water, *J. Geophys. Res.*, *107*(E12), 5128, doi:10.1029/2001JE001809.

Lallement, R., J. L. Bertaux, and F. Dalaudier (1985), Interplanetary Lyman-alpha spectral profiles and intensities for both repulsive and attractive solar force fields: Predicted absorption pattern by a hydrogen cell, *Astron. Astrophys.*, *150*, 21–32.

Levine, J. S., D. S. McDougal, D. E. Anderson, and E. S. Barker (1978), Atomic hydrogen on Mars: Measurements at solar minimum, *Science*, *200*(4345), 1048–1051.

Matta, M., P. Withers, and M. Mendillo (2013), The composition of Mars' topside ionosphere: Effects of hydrogen, *J. Geophys. Res. Space Physics*, *118*, 2681–2693, doi:10.1002/jgra.50104.

McClintock, W. E., N. M. Schneider, G. M. Holsclaw, J. T. Clarke, A. C. Hoskins, I. Stewart, F. Montmessin, R. V. Yelle, and J. Deighan (2014), The Imaging Ultraviolet Spectrograph (IUVS) for the MAVEN mission, *Space Sci. Rev.*, doi:10.1007/s11214-014-0098-7.

Nair, H., M. Allen, A. D. Anbar, Y. L. Yung, and R. T. Clancy (1994), A photochemical model of the Martian atmosphere, *Icarus*, *111*, 124–150.

Quémerais, E., B. R. Sandel, V. V. Izmodenov, and G. R. Gladstone (2013), Thirty years of interplanetary background data: A global view, in *Cross-Calibration of Far UV Spectra of Solar System Objects and the Heliosphere*, edited by E. Quémerais, M. Snow, and R.-M. Bonnet, pp. 141–162, Springer, New York.

Snow, M., A. Reberac, E. Quémerais, J. Clarke, W. E. McClintock, and T. N. Woods (2013), A new catalog of ultraviolet stellar spectra for calibration, in *Cross-Calibration of Far UV Spectra of Solar System Objects and the Heliosphere*, edited by E. Quémerais, M. Snow, and R.-M. Bonnet, pp. 191–226, Springer, New York.

Thomas, G. E. (1963), Lyman α scattering in the Earth's hydrogen geocorona: 1, *J. Geophys. Res.*, *68*, 2639–2660.

Valeille, A., V. Tenishev, S. W. Bougher, M. R. Combi, and A. F. Nagy (2009), Three-dimensional study of Mars upper thermosphere/ionosphere and hot oxygen corona: 1. General description and results at equinox for solar low conditions, *J. Geophys. Res.*, *114*, E11005, doi:10.1029/2009JE003388.

Verigin, M. I., K. I. Gringauz, G. A. Kotova, N. M. Shutte, H. Rosenbauer, S. Livi, A. K. Richter, W. Riedler, K. Schwingenschuh, and K. Szego (1991), On the problem of the Martian atmosphere dissipation: Phobos 2 TAUS spectrometer results, *J. Geophys. Res.*, *96*(A11), 19,315–19,320.

Villanueva, G. L., M. J. Mumma, R. E. Novak, H. U. Kaufl, P. Hartogh, T. Encrenaz, A. Tokunaga, A. Khayat, and M. D. Smith (2015), Strong water isotopic anomalies in the Martian atmosphere: Probing current and ancient reservoirs, *Science*, *348*(6231), 218–221.

Zahnle, K., R. M. Haberle, D. C. Catling, and J. F. Kasting (2008), Photochemical instability of the ancient Martian atmosphere, *J. Geophys. Res.*, *113*, E11004, doi:10.1029/2008JE003160.